Check for updates

Chirality dependent inverse-melting and re-entrant gelation in α-cyclodextrin/1-phenylethylamine mixtures†

Reut Shapira, Sapir Katalan, Rachel Edrei and Yoav Eichen ⓘ *

Solutions of cyclohexakis-(1→4)-α-ᴅ-glucopyranosyl, α-cyclodextrin, αCD, in *R*-(+)-1-phenylethylamine, αCD/R-PEA, and *S*-(−)-1-phenylethylamine, αCD/S-PEA, display abnormal phase transitions that strongly depend on supramolecular diastereomeric interactions. While αCD/R-PEA mixtures show one sol–gel inverse-melting phase transition, αCD/S-PEA mixtures show temperature dependent gel–sol–gel re-entrant behavior. NMR, Raman spectroscopy, microscopy and X-ray scattering measurements reveal that hydrogen bond weakening in solution, as well as changes in crystal composition are responsible for entropy increase and gel formation upon heating.

Introduction

Re-entrant phase transitions occur when a continuous thermodynamic field variation, usually temperature or pressure, shows two or more phase transitions, and the final state *visually resembles* the initial state.[1] In such cases, it looks as if the system returns to, or "re-enters", its original state. However, even though the initial and final states are macroscopically similar, thermodynamics dictates that these two phases must be different, in either composition or structure. This abnormal phase behaviour is one of few less common phase transitions, of which the anomaly of water in the temperature–pressure–volume space is most known and studied.[2–4] Yet another anomalous phase transition, sometimes found in mixtures, is inverse-melting, also referred to as inverse-freezing,[5,6] describing a liquid solution that reversibly solidifies upon heating, and melts upon cooling. Recently, these odd phase transitions draw attention because of their relevance to biology[7–9] and different fields of technology.[10–13]

In a recent publication,[14] we have reported on our efforts to gain understanding of the microscopic picture of inverse melting in mixtures of low molecular weight components. The work focused on inverse melting solutions of cyclohexakis-(1→4)-α-ᴅ-glucopyranosyl, α-cyclodextrin, αCD, a cyclic hexamer of ᴅ-glucopyranose linked to one another through α-1,4 glycosidic bonds, in aqueous pyridine.[15–18] As some water–pyridine mixtures are known to show re-entrant phase behavior,[19,20] we explored the possibility that the similarities between re-entrant transitions and inverse melting processes are non-coincidental.

NMR studies of these systems revealed surprising relationship between inverse-melting and re-entrant supramolecular interactions in the solvent, implying that these two processes are linked to one another.[14] In phase transitions that involve formation of solids, re-entrant phase transition, or at least re-entrant intermolecular interactions, could be a pre-requisite for the appearance of inverse melting.[14]

Phase re-entrance phenomena are sometimes observed in binary liquid solutions[1,21,22] and gases,[23–25] denaturation of proteins,[26–28] liquid crystals,[29–31] and gels.[32–36] This abnormal phase behaviour was first observed over 100 years ago.[22] However, despite its role in important fields of biology and technology,[7,9,12,13] it received relatively limited attention, mainly from physicists who developed models that put this phenomenon in the right thermodynamics perspective.[37–39] In contrast, there is only very limited success in revealing the supramolecular origins of this phenomenon.[40–42]

Focusing on re-entrant gel transitions, most of the known formulations are based on high-molecular-weight polymers, composed of mixtures of at least three components.[33–35] The presence of polymers in many of the inverse freezing and re-entrant systems is not surprising. Due to their length and wealth of degrees of freedom, polymers have many possible conformations, of which some are enthalpy favoured, while others are populated only at higher temperatures, invoking entropy into play. Therefore, a system containing a polymer has a better chance to exhibit re-entrant gel formation compared to a mixture of small molecules, with limited number of conformations.

The present paper focuses on a new system that is composed of two chiral low-molecular weight components: αCD and different proportions of the two enantiomers of 1-phenylethylamine, PEA. Similar to the systems reported by Zheng *et al.*,[43–45] we expected that diastereomeric interactions between enantiopure αCD and the two enantiomers of PEA will result in notably

Schulich Faculty of Chemistry, Technion – Israel Institute of Technology, Technion City, 3200008 Haifa, Israel. E-mail: yoav@ch.technion.ac.il

† Electronic supplementary information (ESI) available. See DOI: 10.1039/d0ra07643k

different macroscopic phase diagrams for the two systems. Indeed, a re-entrant gel is formed upon mixing αCD with pure S-(−)-PEA. In contrast, under the same conditions, mixtures of αCD and R-(+)-PEA show only inverse melting behaviour. The phase diagram, as well as the structural and thermal properties of αCD/PEA mixtures were characterized using viscometry, light transmittance, differential scanning calorimetry, NMR, Raman spectroscopy, optical and electron microscopy and X-ray scattering techniques, all in order to obtain understanding of this unique system.

Results and discussion

Molecule structures

At room temperature a mixture of 0.25 gr of αCD in 1 ml of (R)-(+)-PEA, αCD/R-PEA, is a clear, fluid and homogeneous solution. The solution contains about 1.1% wt water, and the mole ratio of the components is $1 : 30 : 3$ αCD : (R)-(+)-PEA : H_2O. In contrast, at the same temperature, a similar mixture of 0.25 g αCD in 1 ml of (S)-(−)-PEA ($1 : 30 : 3$ αCD : (S)-(−)-PEA : H_2O), αCD/S-PEA, appears as a highly viscous, opaque microcrystalline gel. Clearly, the difference between the two systems stems from diastereomeric differences in the supramolecular interactions between αCD and the two PEA enantiomers, yielding

chirality dependent match and miss-match between the solvent, PEA, and the solute, αCD.[46] This difference in matching is also revealed from the difference in the association constant between αCD and PEA enantiomers observed in aqueous solutions, $K_{ass} = 26.0$ and 33.6 L mol^{-1} for R-(+)-PEA and S(−)-PEA respectively.[47] Moreover, because of this difference in intermolecular interactions, cyclodextrins were found suitable for separation of enantiomers of PEA.[48–52] For example, a commercially available column, with a stationary phase coated with β-cyclodextrin, βCD, separates R-(+)-PEA from S(−)-PEA in useful resolution, with R-(+)-PEA being eluted first when hydrophobic eluents are used.

Interestingly, upon heating these two mixtures, their behaviour becomes macroscopically similar. At around 65 °C the gel of αCD/S-PEA melts, turning into a homogeneous liquid while αCD/R-PEA retains its homogeneous liquid-state. Upon further heating to above 75 °C, both solutions solidify, forming an inverse melting gel, Fig. 1. These are the only phase transitions one can observe visually in the −10 °C to +100 °C temperature range and atmospheric pressure.

Temperature dependent viscosity of αCD/PEA mixtures

One of the main characteristics of the gel state is its relative high viscosity compared to the fluid liquid-state.[53,54] To support
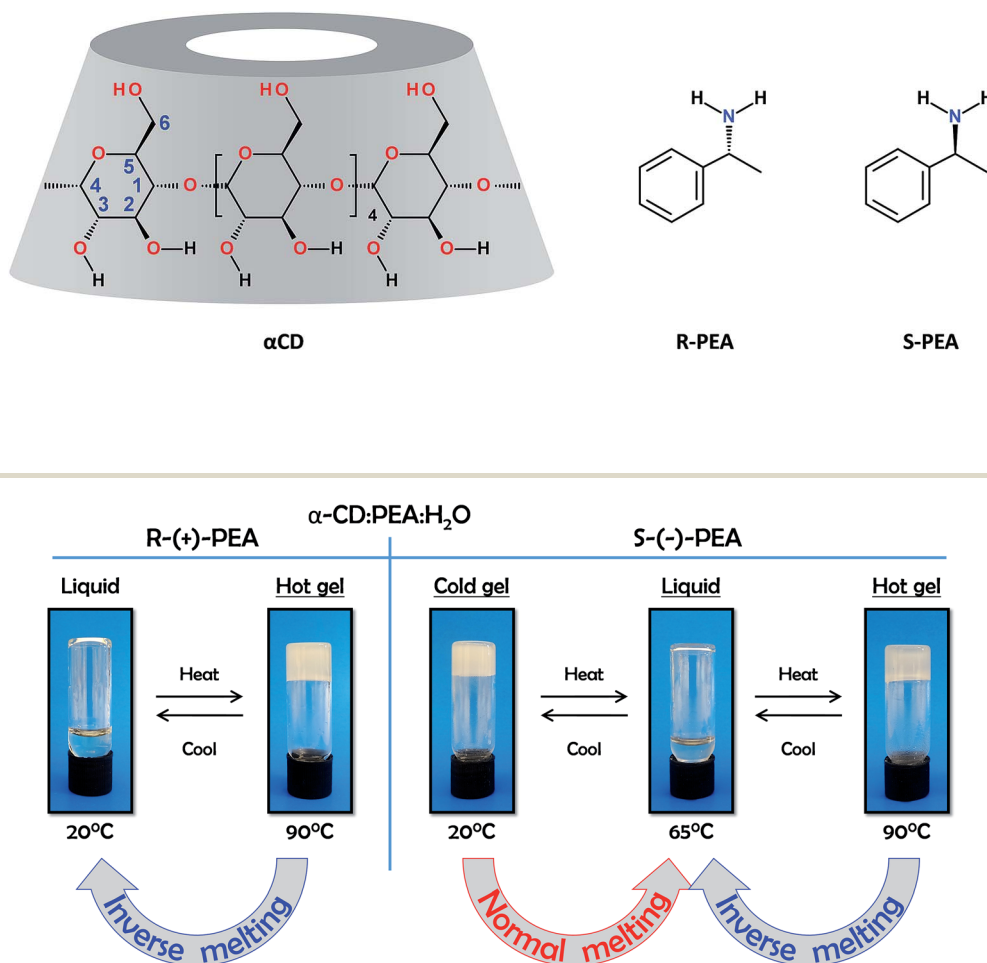

αCD   R-PEA   S-PEA

Fig. 1 Temperature dependent sol–gel phase transitions in αCD/R-PEA (left) and αCD/S-PEA (right) in the −10 to +100 °C temperature range.
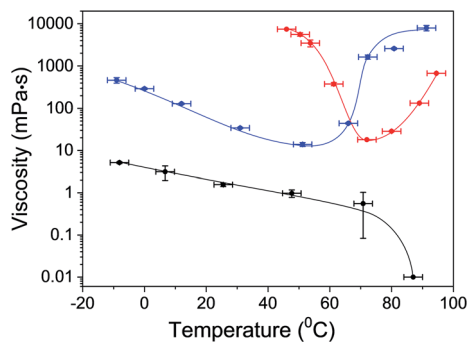
Fig. 2 Viscosity of αCD/R-PEA (blue) and αCD/S-PEA (red) as function of temperature. The viscosity of the pure solvent, PEA, (black) is provided as reference. Error bars were evaluated from the standard deviation of 4–6 measurements taken at each temperature. The error in the temperature domain is ±3 °C. The Maximal detection limit is 10^4 mPa s.

gel formation and extract the gelation points, the viscosity of αCD/R-PEA and αCD/S-PEA was measured as a function of the temperature, Fig. 2. In accordance with the findings presented in Fig. 1, αCD/R-PEA mixture has relatively low viscosity at temperatures below 60 °C, 1–2 order of magnitude higher than pure PEA. The viscosity of the system drops with increasing temperature, resembling pure R-PEA and S-PEA. At temperatures above 60 °C the viscosity increases dramatically with temperature, reaching a highly viscous gel state at about 90 °C.

In contrast, at low temperatures, the viscosity of αCD/S-PEA is very high as the system is in its "cold gel" state. Viscosity starts dropping at about 50 °C as the "cold gel" melts. Upon further temperature increase to about 70 °C the viscosity reaches its lowest value, 18 mPa s, and the solution turns homogeneous and transparent. Upon further increasing the temperature the viscosity again increases with temperature as the system transforms into its "hot gel" state.

Temperature dependent light transmittance of αCD/PEA systems

Temperature dependent light transmittance through samples of αCD/R-PEA and αCD/S-PEA was studied at different αCD concentrations and heating rates in heat-and-cool cycles. Around the gelation points the transmittance changed rapidly from high values, characteristic of liquid phases, to lower values that are characteristic of opaque gel phases. For convenient sample comparison, we have looked for a fitting function that could best represent the gelation process. The poly-crystalline structure of the gels (see Microscopy section below), suggests that the formation of the gel commences with slow continuous nucleation, eqn (1), followed by autocatalytic crystal growth, eqn (2):
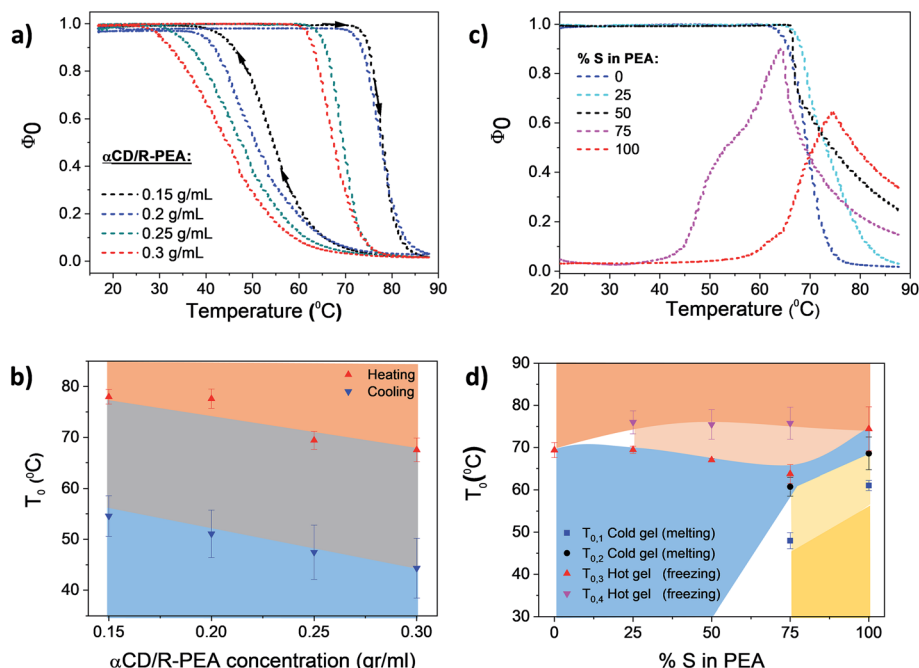
$$A \xrightarrow{k_1} B \tag{1}$$

$$A + B \xrightarrow{k_2} 2B \tag{2}$$

Fig. 3 Transmittance results of αCD/PEA mixtures: (a) normalized transmittance as a function of the temperature of αCD/R-PEA having different αCD concentrations (heat-and-cool cycle, 0.13 °C min⁻¹). (b) αCD/R-PEA sigmoid midpoints T_0 and ΔT (as error bars) for each sample at a heating and cooling rate of 0.13 °C min⁻¹; red rectangle represents the solid gel state, blue rectangle represents the homogeneous liquid state and grey rectangle represents the hysteresis region. (c) Temperature dependent light transmittance of 0.25 g ml⁻¹ αCD/PEA at different enantiomeric excesses for the PEA solvent (heating), (d) 0.25 g ml⁻¹ αCD/PEA sigmoid midpoints T_0 and ΔT (as error bars) for each sample. Light blue: liquid phase, light red and pink: hot gel phases, yellow and light yellow: cold gel phases, white: uncharacterized conditions. Heating rate: 0.13 °C min⁻¹.

where A is the fraction of the molecules in the liquid phase and B is the fraction of the molecules in the crystal phase, k_1 and k_2 are the rate constants of the two steps. Based on the Finke–Watzky model for this two-step process,[55] the transmittance, which is proportional to the gel formation, was fitted to eqn (3):

$$\Phi(T) = (\Phi_0 - p)\frac{k_1 + k_2\phi_0}{k_2\phi_0 + k_1 \ \exp(k_1 + k_2\phi_0 T)} + p \quad (3)$$

where $\Phi(T)$ is the normalized transmittance at temperature T, Φ_0 and p, are constants of the initial and final normalized transmittance values respectively, k_1 is the nucleation rate, and k_2 is the crystal growth rate.

The fitting parameters show that in all of our systems $k_1 \ll k_2\phi_0$, and that the behaviour of the system can be efficiently represented by a simpler sigmoid fitting function, eqn (4):

$$\Phi(T) = (\Phi_0 - p)\frac{1}{1 + \exp\left(\dfrac{T - T_0}{\Delta T}\right)} + p \quad (4)$$

where T_0, is the sigmoid midpoint, which is defined to be the phase transition temperature, and ΔT is the width of the decay region.

Temperature dependent light transmittance of αCD/R-PEA samples at different concentrations of αCD, Fig. 3a and b, showed the presence of only one phase transition in the 20 °C to 90 °C temperature range and results were fitted using eqn (4). Similar to other low molecular weight inverse melting gels,[56] the phase transition temperature, T_0, drops with increasing αCD concentration. Upon heating, T_0 values were found to be 78, 77, 69 and 67 °C for 0.15, 0.2, 0.25 and 0.3 g mol⁻¹ αCD/R-PEA solutions respectively. Cooling the same systems yielded T_0 of 55, 51, 47, 44 °C for 0.15, 0.2, 0.25 and 0.3 g mol⁻¹ αCD/R-PEA solutions respectively, presenting an average hysteresis of 23 °C. The concentration of αCD in the system does not seem to influence the gel structure as the general trend of curve is maintained through all four measured concentrations. Similar curves were built for systems containing S-PEA and mixtures of R-PEA and S-PEA, Fig. 3c and d and S1.† The "cold gel" of αCD/S-PEA melts upon heating in two sequential steps, Fig. 3c, thus a bi-sigmoidal function was applied for fitting the normal melting region, eqn (S1),† represented as $T_{0,1} = 58$ °C and $T_{0,2} = 68$ °C at 100%, S-PEA in Fig. 3d (see Fig. S2 and Table S1† for more details about fitting). At $T_{0,3} = 74$ °C, this sample forms a "hot gel" with low transmittance in an inverse melting transition. The use of different enantiomeric compositions of PEA as the solvent for αCD results with different phase transition profiles. Fig. 3c clearly shows that the system containing αCD and racemic PEA, αCD/rac-PEA (black line), has one liquid-to-gel transition at high temperature, and is macroscopically similar to the αCD/R-PEA system. However, αCD/rac-PEA shows two clear sub-processes in the liquid-to-gel transition ($T_{0,3} = 67$ °C and $T_{0,4} = 75$ °C in Fig. 3d), in contrast to only one process observed for αCD/R-PEA. The first sub-transition for αCD/rac-PEA could be formation of gel structure made of αCD and R-PEA, while the second sub-transition seems to be related to the formation of gel structure made of αCD and S-PEA. This two-step transition is observed also upon heating the αCD/75R:25S-
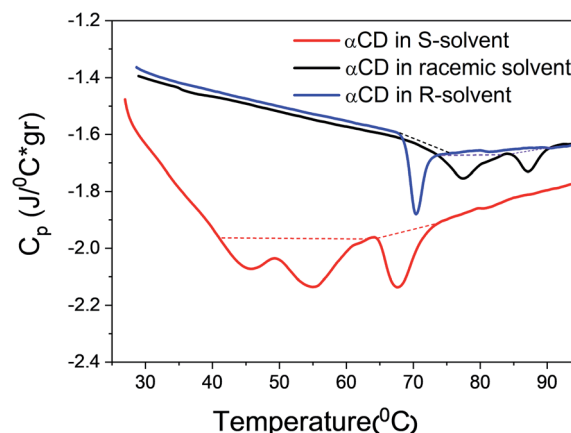

Fig. 4 DSC thermographs of 0.25 g ml⁻¹ αCD/R-PEA (blue), αCD/rac-PEA (black) and αCD/S-PEA (red). Heating rate: 1 °C min⁻¹.

PEA system, cyan line, where the solvent mixture contains more R-PEA than S-PEA. This mixture is characterized by transition temperatures of $T_{0,3} = 69$ °C and $T_{0,4} = 76$ °C. The αCD/25R:75S-PEA system (magenta line) exhibits a curve shape that is similar to αCD/S-PEA and presents two main transitions: "cold gel" to liquid and liquid to "hot gel". However, the "cold gel" of αCD/25R:75S-PEA has lower melting points, $T_{0,1} = 48$ °C and $T_{0,2} = 61$ °C, implying that it is less stable than the "cold gel" of pure αCD/S-PEA. We assume that the disturbance of R-PEA enantiomer to the "cold gel" structure of αCD/25R:75S is responsible for the decrease in the observed melting points. The "hot gel" of αCD/25R:75S-PEA which forms at $T_{0,3} = 63$ °C and $T_{0,4} = 76$ °C, is observed at lower temperature than the "hot gel" of αCD/S-PEA. Here too, two sub transitions are observed due to the presence of two diastereomeric structures of αCD-PEA, as in αCD/rac-PEA and αCD/75R:25S-PEA. Fig. 3d presents the phase transition temperature as a function of the enantiomeric composition of the PEA solvent. All transition temperatures were confirmed independently using numerical first and second derivatives for each transmittance curve.[57] The dependence of the phase transition temperature on heating rate is presented in Fig. S3.†

Differential scanning calorimetry

Thermograms of αCD/R-PEA, αCD/rac-PEA and αCD/S-PEA mixtures were recorded using differential scanning calorimetry, DSC, at a heating rate of 1 °C min⁻¹, Fig. 4. All the transitions found in the thermographs are first-order with $\Delta H = +2.30$ J g⁻¹ for melting of the αCD/S-PEA "cold gel", and $\Delta H = +0.6$ J g⁻¹, 0.82 J g⁻¹ and 0.92 J g⁻¹ for the formation of the "hot gel" of αCD/R-PEA, αCD/rac-PEA and αCD/S-PEA, respectively. Melting of the "cold gel" of αCD/S-PEA as well as the solidification of αCD/rac-PEA upon heating are composed of at least two sub-processes, in agreement with the results obtained from temperature dependent light transmission. The amount of heat consumed during these liquid-to-gel transitions is similar to the previously reported ΔH values for the inverse melting process in αCD/4-MP/H₂O mixtures,[17,58] and two order of magnitude lower than that of water melting. The relatively small ΔH values suggest that the strength of the
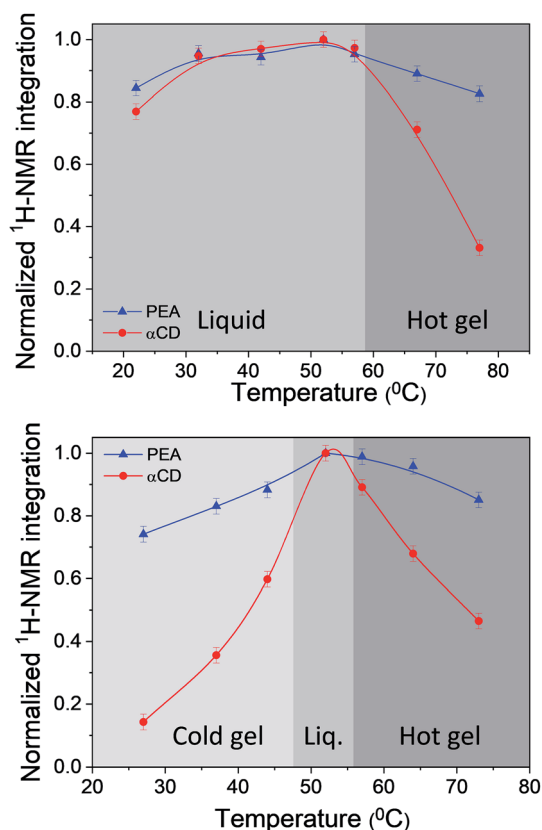
Fig. 5 Normalized ^{1}H-NMR integration values of the solvent PEA methyl peak (blue) and the solute αCD-H1 peak (red) as a function of temperature for 0.25 g ml^{-1}: top: αCD/R-PEA and bottom: αCD/S-PEA.

Fig. 6 Raman spectra of PEA (bottom), αCD/R-PEA (middle) and αCD/S-PEA (top) at different temperatures: 0 °C, 20 °C, 60 °C and 90 °C. Focus on N–H vibrations at ~750 cm^{-1} and 3000 cm^{-1}.

intermolecular interactions does not change dramatically during phase transition, and that the major effect originates from re-ordering of the systems.

NMR spectroscopy

Temperature dependent solution ^{1}H-NMR spectra of αCD/R-PEA and αCD/S-PEA were taken across the thermally induced gelation points, Fig. S4 and S5,† respectively. Relying on the loss of NMR peak intensity one can quantify the percentage of the different components turning anisotropic upon gelation.[14,59] Fig. 5 reveals that while in the liquid phase the integration of the peaks of the different ingredients match the true system composition of 1 : 30 : 3 αCD : PEA : H$_2$O, all gel phases possess significantly lower αCD concentrations, implying that upon gelation most of the αCD separates from solution and participates in the solid network. Moreover, an important difference between the hot and cold gels of the αCD/S-PEA system is that the solid of the "cold gel" consists of a 1 : 9.5 ± 0.5 αCD : S-PEA, consuming about 28% of the PEA and 86% of the αCD of the system, while the solid of the "hot gel" consists of a 1 : 7.5 ± 0.5 αCD : S-PEA, consuming about 14% of the PEA and 54% of the αCD of the system. For the "hot gel" of αCD/R-PEA, the αCD : R-PEA ratio is found to be 1 : 7.5 ± 0.5, similar to the "hot gel" of αCD/S-PEA.

Raman spectroscopy

The counterintuitive material behavior expressed in phase reentrance and inverse melting is often explained by a change in hydrogen bonding upon heating. In the liquid phase of most of such systems, molecules participate in hydrogen bound networks, dictating low orientational entropy. Heating increases the orientational entropy by populating non hydrogen bound states, separation of solid components and formation of a gel. Thus, for gaining more information on the systems reported here, Raman spectroscopy was used for following the temperature dependence of hydrogen bonds in αCD/PEA mixtures. Raman spectra taken at the different temperatures are identical in vibration energy, except in three regions that show important temperature dependence: N–H stretching around 3300 cm^{-1}, N–H deformation around 750 cm^{-1} and broad absorption peak around 400 cm^{-1}, Fig. 6 (full spectra are presented in Fig. S6†). Upon heating pure PEA, the N–H stretching vibration peaks (symmetric and asymmetric bands) shift to higher energy, whereas N–H deformation vibration peaks shifts to lower energy, Fig. 6 bottom, an indication of hydrogen bond weakening.[60] Temperature-dependent Raman spectroscopy of inverse melting αCD/R-PEA, Fig. 6 middle, and re-entrant αCD/S-PEA, Fig. 6 top, show similar effects on N–H stretching and deformation peaks. The results suggest weakening of hydrogen bonds, mainly between solvent molecules, in both αCD/R-PEA and αCD/S-PEA mixtures upon increasing temperature. This contributes to the increase in orientational, and thus total, entropy upon gelation. In all systems the absorption of the N–H stretch vibration is composed of at least two peaks that belong to at least two populations, and their relative intensity changes with temperature. Work is currently directed towards fully characterizing the origins of this temperature dependence and results will be published in due course.

Microscopy

Light microscopy and cryo-scanning electron microscopy (cryo-SEM) were applied to the exploration of the morphological differences between the "cold gel" and "hot gel" of αCD/S-

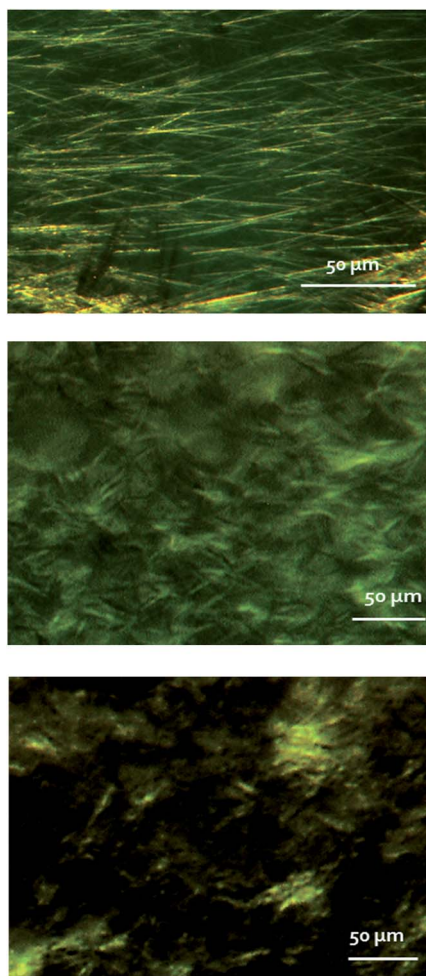Fig. 7 Light microscopy images of αCD/S-PEA cold gel (top), αCD/S-PEA hot gel (middle) and αCD/R-PEA hot gel (bottom).
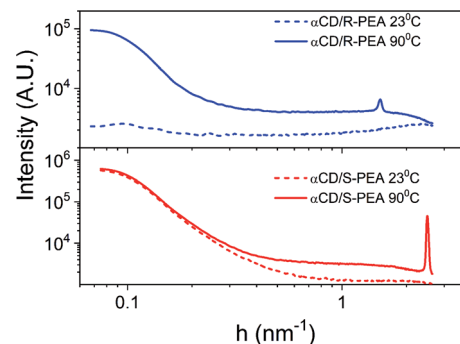

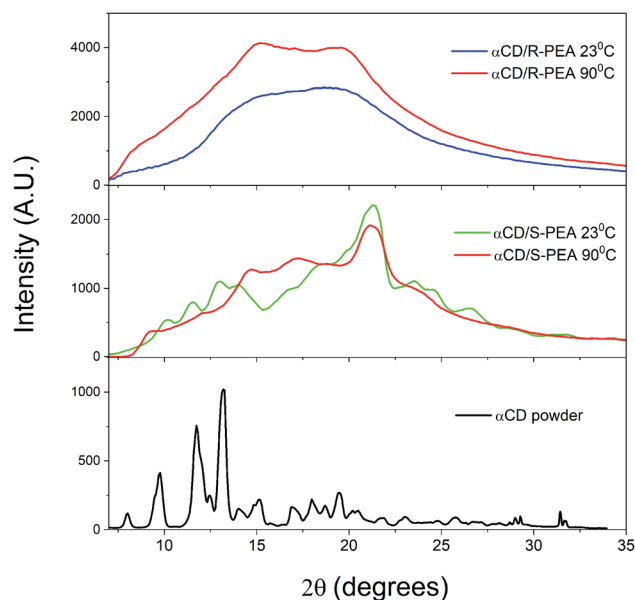Fig. 8 SAXS profiles (log–log scale) of αCD/S-PEA (red) and αCD/R-PEA (blue) at 23 °C and 90 °C.

Fig. 9 WAXS results for αCD powder (bottom, black), αCD/S-PEA at 23 °C (middle, green) and 90 °C (middle, red) and αCD/R-PEA at 23 °C (top, blue) and 90 °C (top, red).

PEA and the "hot gel" of αCD/R-PEA, see Fig. 7 and S7† for light microscopy and cryo-SEM respectively. Both light and cryo-SEM microscopy show clear morphological differences between the three gels. The "cold gel" of αCD/S-PEA consists of long and thin fibres, with a characteristic length of 50–100 μm, and an average width of 1 μm, Fig. 7, top. In contrast, the "hot gel" of αCD/S-PEA appears as an assembly of lamellar layers with average inter-lamellar distance of ∼500 nm, Fig. 7 middle, see also cryo-SEM in Fig. S7† middle. These results agree with the thermodynamic basis of the reentrant phenomena whereby the initial and final states are macroscopically similar but *microscopically* different. Interestingly, the "hot gel" of αCD/R-PEA is morphologically different from the two gels of αCD/S-PEA and is characterized by relatively short, needle-like crystals, with a characteristic length of 1–5 μm and average width of 200 nm.

X-ray scattering

The different crystalline structures of the αCD/R-PEA and αCD/S-PEA gels were also studied using X-ray scattering, providing information about the long-range order of these materials. Fig. 8 shows the normalized SAXS profiles of the αCD/R-PEA and αCD/S-PEA systems at room temperature, 23 °C, and at 90 °C. At room temperature, the solvent, PEA, and liquid αCD/R-PEA show a scattering pattern typical of homogeneous amorphous materials, see blue dashed line in Fig. 8. The "hot gel" of αCD/R-PEA, forming at about 90 °C, shows material inhomogeneity with long-range order characterized by periodicity with $d = 4.13$ nm (peak at $h = 1.522$ nm^{-1}). The presence of distinct diffraction peaks in the diffractogram implies the presence of micron size crystals, see Fig. S8.† The room temperature "cold gel" of αCD/S-PEA shows clear material inhomogeneity with no distinct diffraction peaks, but its "hot gel" shows periodicity with $d = 2.51$ nm ($h = 2.505$ nm^{-1}). All gel-curves were fitted to h^{-4} function, eqn (S2)† showing large-surface particles with background values[61] (fitting results are summarized in Fig. S9†).

Background values indicate the presence of fluid in different amounts that separate the microcrystals in the gel structure. The values are summarized in Table S2† and clearly show that the contribution of the fluid is more dominant in the hot gels than in the cold gel. The fluid is a major contributor to the disorder in the gel structure, so its presence in larger amounts indicates a higher entropy contribution to the higher temperature gels.

Wide angle X-ray scattering, WAXS, was used to compare the unit cells of the crystals of the different gels of αCD/S-PEA and αCD/R-PEA, Fig. 9 and S10.† All gel profiles show broad peaks, indicating the presence of small crystals that are separated by solvent. The WAXS diffraction of a room temperature "cold gel" of αCD/S-PEA, Fig. 9 middle, has three indicative peaks at $2\theta = 11.7, 13.3$ and $14.0°$, which are typical for powders of αCD-hydrate, $\alpha CD \cdot H_2O$, Fig. 9 bottom.[62] These peaks imply that only the "cold gel" of αCD/S-PEA contains the $\alpha CD \cdot H_2O$ inclusion complex, while in the "hot gels" of both αCD/S-PEA and αCD/R-PEA the αCD cavity is either empty or contains a PEA molecule. The release of water molecules from the cavity upon heating joins to other effects mentioned above explaining the entropy gain in the inverse melting process.

Conclusions

Mixtures of αCD/R-PEA and αCD/S-PEA show abnormal inverse-melting and reentrant phase transition, respectively, emphasizing the role of diastereomeric supramolecular interactions in controlling such phase transitions. These mixtures were physically and chemically characterized to understand the origin of their abnormal phase transitions. The different transmittance-based phase diagrams of αCD/R-PEA and αCD/S-PEA exhibit the significant role of 3D fit between solvent and solute in inverse melting systems. According to temperature-transmittance relation and DSC, enantiomeric solvent mixtures show complex transitions that should be more investigated. Characterization of αCD/S-PEA "cold gel" and "hot gel" clearly show that the initial and final phases of the re-entrant system are microscopically different both in structure and composition. NMR and X-ray scattering data show that the gel–sol–gel transition upon heating involves release of PEA and water from the crystals to the fluid, by that increasing the entropy of the system. Raman spectroscopy indicates hydrogen bond weakening upon heating in the PEA solvent itself as a driving force for solidification upon heating, similar to previously reported findings on the αCD/water/4-methylpyridine system.[14] Thus, results show that the temperature dependence of the intermolecular interactions in pure PEA as well as in PEA/water compositions are the main driving force behind these inverse melting and re-entrance phenomena.

Experimental section

Materials

α-Cyclodextrin, αCD, *R*-(+)-phenylethylamine, R-PEA, *S*-(−)-phenylethylamine, S-PEA, were purchased from Sigma-Aldrich and used without further purification.

Sample preparation

αCD/PEA mixtures. 0.15–0.4 g (0.16–0.42 mmol) αCD was dissolved in 1 ml (7.8 mmol) PEA, either enantiomerically pure or a mixture of the two enantiomers. The mixture was heated to 90 °C in a closed vial, reaching its gel phase, and then was allowed to reach room temperature, forming a homogeneous solution (for R-PEA, 50% ee (R-PEA) and racemic-PEA) or an opaque gel (for S-PEA and 50% ee (S-PEA)). All mixtures were used within 7 days from preparation and were stored in closed vials under nitrogen to avoid carbamate formation.[63] Unless otherwise mentioned, the composition of each sample is 0.25 g αCD in 1 ml PEA (containing ∼1.1% w/w water, as measured by Mettler Toledo DL39 Karl Fischer coulometer). The mole ratio of the three components is 1 : 30 : 3 αCD : PEA : H_2O.

Methods

Viscosity. Viscosity was measured using a digital viscometer (SNB-1, Shanghai Nirun Intelligent Technology Co. Ltd., China) with spindles no. 21, 27, 28, 29. Glycerol was used as a reference for calibration, 277 ± 2 mPa s at 40 °C.[64]

Transmittance. Temperature dependent transmittance was recorded using a home-made temperature controlled spectrophotometer composed of a red LED light ($\lambda = 624$ nm), a temperature controlled cuvette holder (−10 °C to 90 °C, Peltier device, heating/cooling rate = 0.13 °C min^{-1}). Data was collected every 20 seconds, and each point was normalized to a reference value of an empty cuvette and then to the maximal transmittance value of the heating–cooling cycle.

Differential scanning calorimetry. DSC measurements were carried out using a DSC1 system equipped with a HSS7 high-sensitivity sensor (Mettler Toledo). Measurements are carried out in closed capsules under a nitrogen atmosphere. Measurements are performed at heating and cooling rates of 10 °C min^{-1}, between 25 °C and 110 °C. All curves reported here were extracted from the last segment of a heating–cooling–reheating process.

NMR spectroscopy. Sample preparation and temperature dependent NMR were reported elsewere.[14]

Raman spectroscopy. Raman spectra were recorded on a confocal micro-Raman LabRam HR instrument (Horiba Scientific) in backscattering geometry with a X50 objective mounted on an Olympus optical microscope. The excitation line was provided by a 532 nm laser (Torus, 100 mW) and a Peltier cooled charge-couple device (CCD) (1024 × 256 pixels) was used as detector. The spectrometer was calibrated using a silicon reference at 520 cm^{-1}, which gives a peak position resolution of about 1 cm^{-1}. Each spectrum is an average of five acquisitions with acquisition time of 30 s. All spectra were baseline corrected for clarity. Sample temperature was controlled using a THMS600 System (Linkam Scientific Instruments).

Light spectroscopy. Inverse melting mixtures were inserted into Borosilicate Capillary Micro Glass Slide 0.20 × 4.0 × 50 mm (Electron Microscopy Sciences) and sealed at both ends using a UHU® 2-K-EPOXIDKLEBER epoxy glue. The samples were studied using a BHS microscope (Olympus) with 5.0 MP Moticam-5 Digital Camera for Microscopes (National Optical &

Scientific Instruments, Inc.) using a X10 and X20 objective for αCD/R-PEA and αCD/S-PEA, respectively. Sample temperature was controlled using a THMS600 System (Linkam Scientific Instruments). Best images were obtained using the scattering mode, with the light source perpendicular to the camera.

Cryo-scanning electron microscopy. Samples for cryo-SEM were cryo-fixed by manual drop plunging. In this method, a 5 µL drop of the relevant gel was set atop a special planchette which was heated to the gelling temperature. Then, the planchette was manually plunged into liquid nitrogen and settled atop a specialized sample table. Exposure of the inner part of the drop was carried out using the BAF060 freeze fracture system by a rapid stroke from a cooled knife. Cryo-SEM imaging were taken according to Koifman et al.[65]

Small-angle X-ray scattering. Small-angle X-ray scattering experiments were performed on a small-angle diffractometer (Molecular Metrology SAXS system) with Cu Kα radiation from a sealed micro-focus tube (MicroMax-002+S), two Göbel mirrors, and three-pinhole slits (Generator powered at 45 kV and 0.8 mA). The scattering patterns were recorded by a 20×20 cm two-dimensional position sensitive wire detector that was positioned 150 cm behind the sample. The resolution of the SAXS system is greater than $\pi/h_{max} = \pi/2.7$, ~1.16 nm.

The scattered intensity $I(h)$ was recorded in the interval 0.07 $< h <$ 2.7 nm^{-1}, where h is the scattering vector defined as $h = (4\pi/\lambda)\sin(\theta)$, 2θ is the scattering angle, and λ is the radiation wavelength (0.1542 nm). The solutions under study were sealed in a glass capillary of about 2 mm in diameter and 0.01 mm wall thickness and measured at 23 and 90 °C under vacuum. $I(h)$ was normalized to time, solid angle, primary beam intensity, capillary diameter, transmission, and the Thompson factor. Scattering of the solvent, empty capillary and electronic noise were subtracted. All calculations were performed using the Mathcad software. All structured element appears again after heating–cooling–heating process.

Wide-angle X-ray scattering. WAXS experiments were performed using the same small/wide-angle diffractometer and Linkam holder. The scattering patterns were recorded by a 15×15 cm two-dimensional imaging plate (BAS-IP-MS, FUJIFILM), positioned about 3 cm behind the sample. The scattering intensity was recorded together with SAXS in interval $5° < 2\theta < 51°$, where 2θ is the scattering angle. Exposition time was ~2 hours. The samples were fixed in cell closed by Mica or polyimide or Al films and placed on a Linkam holder perpendicular to the beam and measured under vacuum at 23 and 90 °C together with SAXS measurement. The imaging plate was scanned by a Fluorescent Image Analysing System (FLA-7000) and analysed by FLA-7000 Image Reader software (version 10) with 100 µm resolution.

Conflicts of interest

Authors state that there are no conflicts to declare.

References

1 T. Narayanan and A. Kumar, *Phys. Rep.*, 1994, **249**, 135–218.

2 Y. D. Fomin, E. N. Tsiok and V. N. Ryzhov, *Eur. Phys. J.: Spec. Top.*, 2013, **216**, 165–173.

3 A. M. Almudallal, S. V. Buldyrev and I. Saika-Voivod, *J. Chem. Phys.*, 2012, **137**, 034507.

4 D. Frenkel, *Phys. A*, 1999, **263**, 26–38.

5 G. P. Johari, *Phys. Chem. Chem. Phys.*, 2001, **3**, 2483–2487.

6 A. L. Greer, *Nature*, 2000, **404**, 134–135.

7 R. Asor, O. Ben-Nun-Shaul, A. Oppenheim and U. Raviv, *ACS Nano*, 2017, **11**, 9814–9824.

8 L. Letamendia and F. J. Bermejo, in *Metastable Systems under Pressure*, ed. S. Rzoska, A. Drozd-Rzoska and V. Mazur, Springer, Odessa, 2010, pp. 153–166.

9 I. Alshareedah, T. Kaur, J. Ngo, H. Seppala, L. A. D. Kounatse, W. Wang, M. M. Moosa and P. R. Banerjee, *J. Am. Chem. Soc.*, 2019, **141**, 14593–14602.

10 Y. Rotbaum, G. Parvari, Y. Eichen and D. Rittel, *Macromolecules*, 2017, **50**, 4817–4826.

11 G. Parvari, Y. Rotbaum, Y. Eichen and D. Rittel, *Chem. Commun.*, 2018, **54**, 12578–12581.

12 K. Senol, G. Parvari, Y. Rotbaum, Y. Eichen, D. Rittel and A. Shukla, *Int. J. Impact Eng.*, 2020, **140**, 103547.

13 J. Zhang, W. Yang, A. Q. Vo, X. Feng, X. Ye, D. W. Kim and M. A. Repka, *Carbohydr. Polym.*, 2017, **177**, 49–57.

14 R. Shapira, Y. S. Balazs, S. Kababya, R. Edrei and Y. Eichen, *Phys. Chem. Chem. Phys.*, 2018, **20**, 29610–29615.

15 M. Plazanet, C. Floare, M. R. Johnson, R. Schweins and H. P. Trommsdorff, *J. Chem. Phys.*, 2004, **121**, 5031–5034.

16 M. Plazanet, M. Dean, M. Merlini, A. Hüller, H. Emerich, C. Meneghini, M. R. Johnson and H. P. Trommsdorff, *J. Chem. Phys.*, 2006, **125**, 1–7.

17 E. Tombari, C. Ferrari, G. Salvetti and G. P. Johari, *J. Chem. Phys.*, 2005, **123**, 051104-1–051104-4.

18 R. Angelini, G. Salvi and G. Ruocco, *Philos. Mag.*, 2008, **88**, 4109–4116.

19 R. J. L. Andon and J. D. Cox, *J. Chem. Soc.*, 1952, 4601.

20 J. D. Cox, *J. Chem. Soc.*, 1952, 4606.

21 J. D. Cox and E. F. G. Herington, *Trans. Faraday Soc.*, 1956, **52**, 926–930.

22 C. S. Hudson, *Z. Phys. Chem.*, 1904, **47**, 113–115.

23 J. A. Schouten, *Phys. Rep.*, 1989, **172**, 33–92.

24 A. Deerenberg, J. A. Schouten and N. J. Trappeniers, *Phys. A*, 1980, **103**, 183–204.

25 R. J. Tufeu, P. H. Keyesg and W. B. Daniels, *Phys. Rev. Lett.*, 1975, **35**, 1004–1006.

26 S. A. Hawley, *Biochemistry*, 1971, **10**, 2436–2442.

27 J. Zhang, X. Peng, A. Jonas and J. Jonas, *Biochemistry*, 1995, **34**, 8631–8641.

28 J. F. Brandts, R. J. Oliveira and C. Westort, *Biochemistry*, 1970, **9**, 1038–1047.

29 P. E. Cladis, D. Guillon, F. R. Bouchet and P. L. Finn, *Phys. Rev. A*, 1981, **23**, 2594–2601.

30 P. E. Cladis, *Phys. Rev. Lett.*, 1975, **35**, 48–51.

31 P. E. Cladis, R. K. Bogardus and D. Aadsen, *Phys. Rev. A*, 1978, **18**, 2292–2306.

32 H. Nagatomi, N. Yanai and N. Kimizuka, *Chem. Lett.*, 2018, **47**, 97–99.

33 S. Katayama, Y. Hirokawa and T. Tanaka, *Macromolecules*, 1984, **17**, 2641–2643.

34 T. Li, T. Ci, L. Chen, L. Yu and J. Ding, *Polym. Chem.*, 2014, **5**, 979–991.

35 F. Bomboi, F. Romano, M. Leo, J. Fernandez-Castanon, R. Cerbino, T. Bellini, F. Bordi, P. Filetici and F. Sciortino, *Nat. Commun.*, 2016, **7**, 1–6.

36 A. F. Kostko, J. L. Harden and M. A. McHugh, *Macromolecules*, 2009, **42**, 5328–5338.

37 N. Schupper and N. M. Shnerb, *Phys. Rev. E: Stat., Nonlinear, Soft Matter Phys.*, 2005, **72**, 1–16.

38 M. Sellitto, *Phys. Rev. B: Condens. Matter Mater. Phys.*, 2006, **73**, 1–4.

39 Y. V. Kalyuzhnyi, A. Jamnik and P. T. Cummings, *Soft Matter*, 2017, **13**, 1156–1160.

40 G. Jancsó, *J. Solution Chem.*, 2006, **35**, 991–1005.

41 L. Almásy, P. Bánki, M. C. Bellissent-Funel, M. Bokor, L. Cser, G. Jancsó, K. Tompa and J. M. Zanotti, *Appl. Phys. A: Mater. Sci. Process.*, 2002, **74**, 516–518.

42 W. Marczak, K. Kiełek, B. Czech, H. Flakus and M. Rogalski, *Phys. Chem. Chem. Phys.*, 2009, **11**, 2668–2678.

43 J. L. Zhou, X. J. Chen and Y. S. Zheng, *Chem. Commun.*, 2007, 5200–5202.

44 D. M. Li and Y. S. Zheng, *Chem. Commun.*, 2011, **47**, 10139–10141.

45 Y. S. Zheng, S. Y. Ran, Y. J. Hu and X. X. Liu, *Chem. Commun.*, 2009, 1121–1123.

46 C. Reichardt, *Solvents and Solvent Effects in Organic Chemistry*, Wiley, Weinheim, 3rd edn, 2003.

47 A. Cooper and D. D. MacNicol, *J. Chem. Soc., Perkin Trans. 2*, 1978, 760–763.

48 M. D. Truppo and N. J. Turner, *Org. Biomol. Chem.*, 2010, **8**, 1280–1283.

49 D. W. Armstrong, L. W. Chang and S. S. C. Chang, *J. Chromatogr. A*, 1998, **793**, 115–134.

50 J. Berglund, L. Cedergren and S. B. Andersson, *Int. J. Pharm.*, 1997, **156**, 195–200.

51 W. X. Huang, H. Xu, S. D. Fazio and R. V. Vivilecchia, *J. Chromatogr. B: Biomed. Sci. Appl.*, 1997, **695**, 157–162.

52 X. Y. Gong and P. C. Hauser, *J. Chromatogr. A*, 2005, **1094**, 196–199.

53 H. Henning Winter, *Encycl. Polym. Sci. Technol.*, 2003, **10**, 132–145.

54 M. Djabourov, *Polym. Int.*, 1991, **25**, 135–143.

55 L. Bentea, M. A. Watzky and R. G. Finke, *J. Phys. Chem. C*, 2017, **121**, 5302–5312.

56 P. Terech and R. G. Weiss, *Chem. Rev.*, 1997, **97**, 3133–3159.

57 M. K. Bain, M. Bhowmik, D. Maity, N. K. Bera, S. Ghosh and D. Chattopadhyay, *J. Appl. Polym. Sci.*, 2010, **118**, 631–637.

58 C. Ferrari, E. Tombari, G. Salvetti and G. P. Johari, *J. Chem. Phys.*, 2007, **126**, 2–6.

59 B. Escuder, M. LLusar and J. F. Miravet, *J. Org. Chem.*, 2006, **71**, 7747–7752.

60 P. J. Larkin, *Infrared and Raman Spectroscopy*, Elsevier Inc., The Netherlands, 1st edn, 2011.

61 O. Glatter and O. Kratky, *Small Angle X-ray Scattering*, Academic Press Inc., London, 1982.

62 Y. Nakai, K. Yamamoto, K. Terada, A. Kajiyama and I. Sasaki, *Chem. Pharm. Bull.*, 1986, **34**, 2178–2182.

63 P. Kang, K. M. Lee, W. K. Lee, K. H. Lee, B. Lee, J. Cho and N. H. Hur, *RSC Adv.*, 2014, **4**, 46203–46207.

64 J. B. Segur and H. E. Oberstar, *Ind. Eng. Chem.*, 1951, **43**, 2117–2120.

65 N. Koifman, I. Biran, A. Aharon, B. Brenner and Y. Talmon, *J. Struct. Biol.*, 2017, **198**, 177–185.